






Article

Helmholtz–Galerkin Technique in Dipole Field Scattering from Buried Zero-Thickness Perfectly Electrically Conducting Disk

Mario Lucido ^{1,*}, Giovanni Andrea Casula ², Gaetano Chirico ¹, Marco Donald Migliore ¹,
Daniele Pinchera ¹ and Fulvio Schettino ¹

¹ Department of Electrical and Information Engineering, University of Cassino and Southern Lazio, 03043 Cassino, Italy; gaetano.chirico@studentmail.unicas.it (G.C.); mdmiglio@unicas.it (M.D.M.); pinchera@unicas.it (D.P.); schettino@unicas.it (F.S.)

² Department of Electrical and Electronic Engineering, University of Cagliari, 09124 Cagliari, Italy; andrea.casula@unica.it

* Correspondence: lucido@unicas.it

Abstract: Non-invasive concealed object detection, identification, and discrimination have been of interest to the research community for decades due to the needs to preserve infrastructures and artifacts, guarantee safe conditions for the detection and location of landmines, etc. A modern approach is based on the use of an unmanned aerial vehicle equipped with ground-penetrating radar, which has the advantage of not requiring direct contact with the ground. Moreover, high-resolution underground images are obtained by coherently combining measurements by using a synthetic aperture radar algorithm. Due to the complexity of the real scenario, numerical analyses have always been welcomed to provide almost real-time information to make the best use of the potential of such kinds of techniques. This paper proposes an analysis of the scattering from a zero-thickness perfectly electrically conducting disk buried in a lossy half-space surrounded by air and illuminated by a field generated by a Hertzian dipole located in the air. It is carried out by means of a generalized form of the analytically regularizing Helmholtz–Galerkin technique, introduced and successfully applied by the authors to analyze the plane-wave scattering from a disk and a holed plane in a homogeneous medium. As clearly shown in the numerical results, the proposed method is very effective and drastically outperforms the commercial software CST Microwave Studio 2023.

Keywords: Helmholtz–Galerkin technique; buried disk; Hertzian dipole



Citation: Lucido, M.; Casula, G.A.; Chirico, G.; Migliore, M.D.; Pinchera, D.; Schettino, F. Helmholtz–Galerkin Technique in Dipole Field Scattering from Buried Zero-Thickness Perfectly Electrically Conducting Disk. *Appl. Sci.* **2024**, *14*, 5544. <https://doi.org/10.3390/app14135544>

Academic Editor: Atsushi Mase

Received: 14 May 2024

Revised: 24 June 2024

Accepted: 24 June 2024

Published: 26 June 2024



Copyright: © 2024 by the authors. Licensee MDPI, Basel, Switzerland. This article is an open access article distributed under the terms and conditions of the Creative Commons Attribution (CC BY) license (<https://creativecommons.org/licenses/by/4.0/>).

1. Introduction

Non-invasive concealed object detection, identification, and discrimination have been of interest to the research community for decades due to the need for preserving infrastructures or ancient ruins and artifacts from invasive excavations, with a further advantage in terms of time and costs reduction; or, in war or post-war scenarios, to guarantee safety conditions for the detection and location of landmines in order to avoid devastation and human tragedy caused by explosions due to accidental contact, to name some examples. Among the wide number of approaches developed, those that deserve to be cited are electromagnetic induction, nuclear quadrupole resonance, thermal imaging, and, above all, the techniques based on ground penetrating radar (GPR), which has been widely used in landmine detection (see [1] and the references therein for an overview).

A modern and very effective means to address this problem is based on the use of an unmanned aerial vehicle, i.e., a drone, equipped with GPR [2–5], which, unlike classic techniques based on a hand-operated metal detector or GPR mounted on a dragged trolley, has the advantage of not requiring direct contact with the ground. Moreover, high-resolution underground images can be obtained by coherently combining the measurements by means of a synthetic aperture radar algorithm [6], and it can be easily conceived that the

adoption of modern array configurations for the transmitting and receiving antennas could further improve system performance [7].

Due to the complexity of real scenarios, suitable modeling of the problem is needed to perform numerical simulations that could efficiently provide useful information to best utilize the potential of such kinds of non-invasive techniques. Despite the huge number of techniques based on the finite element method [8], the finite-difference time-domain method [9,10], and the conjugate gradient method [11,12], to cite the most important ones, when dealing with finite scatterers in unbounded media, integral equation formulations are largely preferred because the unknowns and the boundary conditions from which the equations originate are defined on finite supports [13–16].

Since no closed form solution is available for the obtained integral equation, discretization of the integral operator is needed. However, due to the singular nature of the integral equation at hand, the existence of the solution cannot be generally stated, and even more, if such a solution exists, the convergence of a general discretization scheme cannot be demonstrated. Several techniques, collectively called methods of analytical regularization [17], have been developed to overcome these problems. The rationale is to convert the integral equation at hand to a Fredholm second-kind equation by suitably inverting the most singular part of the integral operator. Of course, based on the problem at hand, the integral operator to be inverted can be conveniently identified with the static part, the high-frequency contribution, a suitable canonical problem, and so on. The well-behaved nature of the equation thus obtained is demonstrated by the Fredholm theory, which allows to establish the existence of a solution from its uniqueness and, moreover, the asymptotic convergence of a discretization scheme preserving the nature of the equation to the exact solution of the problem [18]. In principle, there are no reasons to think of regularization and discretization as two consecutive steps. As a matter of fact, they can proceed “hand to hand” by adopting, for example, the Nystrom discretization technique [19–21], which leads to guaranteed-convergence numerical codes founded on the theorems of the quadrature approximations of singular integrals; or the method of analytical preconditioning (MAP) [22], in which Galerkin projection acts as a perfect preconditioner in case a set of orthonormal eigenfunction of the most singular part of the integral operator is selected as expansion basis, thus leading to a Fredholm second-kind matrix equation.

The aim of this paper is to present, for the first time, an analysis of the field scattered from a zero-thickness perfectly electrically conducting (PEC) disk buried in a lossy half-space, surrounded by air, and illuminated by the field generated by a Hertzian dipole located in the air. It is conducted by means of a suitable generalization of the analytically regularizing Helmholtz–Galerkin technique, previously introduced and successfully applied by the authors to the analysis of the plane-wave scattering from a disk [23] and a holed plane [24] in a homogeneous medium. The problem is formulated as an electric field integral equation (EFIE) in the Fourier transform domain for the unknown spectral counterpart of the surface current density on the disk, obtained by imposing vanishing of the tangential to the disk component of the total electric field, i.e., the superposition of the electric field radiated by the dipole and the one scattered from the disk in a planar layered medium. Due to the revolution symmetry of the problem, all the involved functions can be conveniently expanded in a Fourier series and the EFIE recast as an integral equation in the vector Hankel transform (VHT) domain [25]. As a result, the scattered field can be rewritten as the superposition of a free-space contribution, frequently called a “primary” contribution because it contains the most singular part of the integral operator, and a scattered or “secondary” contribution related to the layering of the medium. Since the VHT transforms of the surface curl-free contribution and the surface divergence-free contribution of the general azimuthal harmonic of the surface current density are scalar functions, such contributions are conveniently selected as new unknowns. MAP is used to discretize the integral equation, thus leading to a Fredholm second-kind matrix equation. It is worth noting that the selected basis functions have some additional properties that deserve to be mentioned. First, the guaranteed convergence is fast because the considered basis functions

reconstruct the physical behavior of the surface current density at the edge and around the center of the disk. Second, the convolution integrals resulting from the Galerkin projection reduce to algebraic products since the basis functions admit closed-form spectral domain counterparts, i.e., the matrix coefficients are 1-D improper integrals that, in the worst cases, can be efficiently evaluated by means of an analytical technique developed by the authors in a previous paper [26].

This paper is organized as follows: After this Introduction Section, the formulation of the problem and the proposed solution are presented in Section 2. Section 3 is devoted to showing the fast convergence of the proposed method, to the validation of the developed in-house C++ software code by means of comparisons with CST Microwave Studio 2023 (CST-MWS), and to the reconstruction of the scattered field behavior. The conclusions are summarized in Section 4.

2. Formulation of the Problem and Proposed Solution

2.1. Formulation of the Problem

Figure 1 shows the geometry of the problem: a zero-thickness PEC disk of radius a buried at depth d in a homogeneous and isotropic lossy half-space, called medium 2, surrounded by a half-space filled with air, i.e., medium 1. The symbols ϵ_i and μ_i denote, respectively, the dielectric permittivity and the magnetic permeability of the i -th medium. A Cartesian coordinate system is introduced such that the xy plane and the z axis coincide, respectively, with the flat interface and the disk axis. An arbitrarily oriented Hertzian dipole located in air, of current density $\underline{J}^{\text{inc}}(\underline{r}) = \underline{J}_0 \delta(\underline{r} - \underline{r}_0)$, where $\underline{r} = (x, y, z)$ and $\underline{r}_0 = (x_0, y_0, z_0)$ are the vector positions of the observation point and the dipole, respectively, and $\delta(\cdot)$ is the Dirac delta function, radiates an electromagnetic field, $(\underline{E}^{\text{inc}}(\underline{r}), \underline{H}^{\text{inc}}(\underline{r}))$, thus exciting a surface current density on the disk, $\underline{J}(x, y)$, that in turn generates a scattered field, $(\underline{E}^{\text{sc}}(\underline{r}), \underline{H}^{\text{sc}}(\underline{r}))$. The induced surface current density is related to the jump across the disk of the tangential component of the scattered magnetic field, whereas the incident and scattered electric fields are related to each other by the boundary conditions on the disk surface, i.e.,

$$\underline{J}(x, y) = \hat{z} \times (\underline{H}^{\text{sc}}(x, y, -d^+) - \underline{H}^{\text{sc}}(x, y, -d^-)), \tag{1a}$$

$$\hat{z} \times (\underline{E}^{\text{inc}}(x, y, -d) + \underline{E}^{\text{sc}}(x, y, -d)) = 0, \tag{1b}$$

for $x^2 + y^2 \leq a^2$.

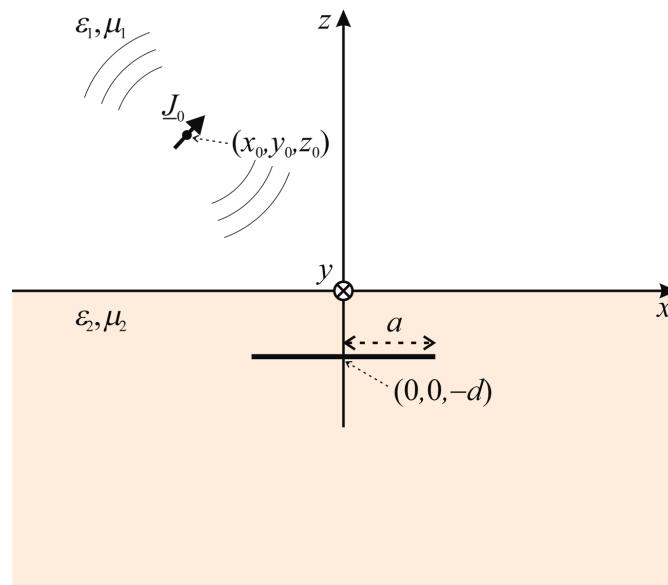


Figure 1. Geometry of the problem.

Hence, a boundary value problem for the Maxwell equation is established. By further imposing the Silver–Muller radiation condition and the power-boundedness condition, the uniqueness of the solution, if it exists, is guaranteed.

Since both the incident and scattered electric fields can be represented by the convolution integral involving the dyadic Green’s function of the problem at hand and the corresponding current density, the Silver–Muller radiation condition is automatically satisfied by the proper selection of Green’s function. Moreover, because Green’s function of a planar layered medium can be expressed in closed form only in the spectral domain [27,28], the incident and scattered electric fields can be conveniently retrieved by means of the inverse Fourier transform of the corresponding spectral domain counterparts.

In general, the electric field generated in medium $i = 1, 2$ by a current density of the kind $\tilde{J}_j(\underline{r}) = \underline{J}_j(x, y)\delta(z - z_j)$ located in medium $j = 1, 2$ can be written as the superposition of a primary or free-space contribution, arising only for $i = j$, and a secondary or scattered contribution, related to the layering of the medium [29], i.e.,

$$\underline{E}_{i,j}(\underline{r}) = \underline{E}_{i,j}^{(P)}(\underline{r}) + \underline{E}_{i,j}^{(S)}(\underline{r}), \tag{2a}$$

$$\underline{E}_{i,j}^{(P)}(\underline{r}) = \begin{cases} \iint_{-\infty}^{+\infty} \underline{\underline{G}}_{i,j}^{(P)}(u, v) \tilde{J}_j(u, v) e^{-j(ux+vy+R_j(u,v)|z-z_j|)} dudv & i = j \\ 0 & i \neq j \end{cases}, \tag{2b}$$

$$\underline{E}_{i,j}^{(S)}(\underline{r}) = \iint_{-\infty}^{+\infty} \underline{\underline{G}}_{i,j}^{(S)}(u, v) \tilde{J}_j(u, v) e^{-j(ux+vy+R_i(u,v)|z|+R_j(u,v)|z_j|)} dudv, \tag{2c}$$

where the following definition of a double Fourier transform has been used:

$$\tilde{f}(u, v) = \frac{1}{4\pi^2} \iint_{-\infty}^{+\infty} f(x, y) e^{j(ux+vy)} dx dy \Leftrightarrow f(x, y) = \iint_{-\infty}^{+\infty} \tilde{f}(u, v) e^{-j(ux+vy)} dudv, \tag{3}$$

and

$$\underline{\underline{G}}_{i,j}^{(T)}(u, v) = \begin{pmatrix} v^2 A_{i,j}^{(T)}(u, v) + u^2 B_{i,j}^{(T)}(u, v) & uv \left(B_{i,j}^{(T)}(u, v) - A_{i,j}^{(T)}(u, v) \right) & u C_{i,j}^{(T)}(u, v) \\ uv \left(B_{i,j}^{(T)}(u, v) - A_{i,j}^{(T)}(u, v) \right) & u^2 A_{i,j}^{(T)}(u, v) + v^2 B_{i,j}^{(T)}(u, v) & v C_{i,j}^{(T)}(u, v) \\ u \bar{C}_{i,j}^{(T)}(u, v) & v \bar{C}_{i,j}^{(T)}(u, v) & D_{i,j}^{(T)}(u, v) \end{pmatrix}, \tag{4a}$$

$$A_{i,j}^{(T)}(u, v) = -\frac{\omega\mu_j}{2R_j(u, v)(u^2 + v^2)} \begin{cases} 1 & T = P \\ T_{i,j}^{(\mu)}(u, v) & T = S' \end{cases} \tag{4b}$$

$$B_{i,j}^{(T)}(u, v) = -\frac{R_i(u, v)}{2\omega\varepsilon_i(u^2 + v^2)} \begin{cases} 1 & T = P \\ T_{i,j}^{(\varepsilon)}(u, v) & T = S' \end{cases} \tag{4c}$$

$$C_{i,j}^{(T)}(u, v) = \frac{R_i(u, v)}{2\omega\varepsilon_i R_j(u, v)} \begin{cases} \text{sgn}(z - z_j) & T = P \\ (-1)^j T_{i,j}^{(\varepsilon)}(u, v) & T = S' \end{cases} \tag{4d}$$

$$\bar{C}_{i,j}^{(T)}(u, v) = \frac{1}{2\omega\varepsilon_i} \begin{cases} \text{sgn}(z - z_j) & T = P \\ (-1)^j T_{i,j}^{(\varepsilon)}(u, v) & T = S' \end{cases} \tag{4e}$$

$$D_{i,j}^{(T)}(u, v) = \frac{u^2 + v^2}{2\omega\varepsilon_i R_j(u, v)} \begin{cases} -1 + j \frac{2R_j(u, v)}{u^2 + v^2} \delta(z - z_j) & T = P \\ (-1)^{j-i} T_{i,j}^{(\varepsilon)}(u, v) & T = S' \end{cases} \tag{4f}$$

$$T_{ij}^{(\eta)}(u, v) = \frac{2\eta_{3-j}R_j(u, v)}{\eta_1R_2(u, v) + \eta_2R_1(u, v)} - \delta_{i,j}, \tag{4g}$$

$$R_i(u, v) = \sqrt{k_i^2 - u^2 - v^2}, \tag{4h}$$

where $\text{sgn}(\cdot)$ is the signum function, $\delta_{m,n}$ is the Kronecker delta, $k_i = \omega\sqrt{\epsilon_i\mu_i}$ is the wavenumber of the i -th medium, and ω is the angular frequency.

By using Equation (2) in Equation (1b), the boundary value problem at hand is recast as an integral equation for the Fourier transform of the surface current density on the disk, i.e.,

$$\begin{aligned} & \int_{-\infty}^{+\infty} \left[\underline{\underline{\mathbf{G}}}_{2,2}^{(P)}(u, v) + \underline{\underline{\mathbf{G}}}_{2,2}^{(S)}(u, v)e^{-j2R_2(u,v)d} \right] \underline{\underline{\mathbf{J}}}(u, v)e^{-j(ux+vy)} dudv \\ &= -\frac{1}{4\pi^2} \int_{-\infty}^{+\infty} \int_{-\infty}^{+\infty} \underline{\underline{\mathbf{G}}}_{2,1}^{(S)}(u, v)e^{-j[u(x-x_0)+v(y-y_0)+R_2(u,v)d+R_1(u,v)z_0]} dudv \underline{\underline{\mathbf{J}}}_0, \end{aligned} \tag{5}$$

for $x^2 + y^2 \leq a^2$, where the dyad $\underline{\underline{\mathbf{G}}}_{i,j}^{(T)}$ (\cdot) is made up of the first two rows of $\underline{\underline{\mathbf{G}}}_{i,j}^{(T)}(u, v)$.

The uniqueness of the solution of (5), if it exists, can be stated by the proper selection of the functional space in which the unknown surface current density has to be searched for. For this purpose, it is worth remembering that, in order to satisfy the power boundedness condition, the components of the surface current density parallel and orthogonal to the edge of a PEC planar scatterer behave at most like $t^{-1/2}$ and $t^{1/2}$, respectively, as the distance t from the edge approaches zero [30,31].

On the other hand, Equation (5) can be deeply simplified by taking advantage of the azimuthal symmetry of the geometry at hand. As a matter of fact, the surface current density on the disk can be conveniently expanded in a Fourier series,

$$\underline{\underline{\mathbf{J}}}(x, y) = \sum_{n=-\infty}^{+\infty} \underline{\underline{\mathbf{J}}}^{(n)}(\rho)e^{jn\phi}, \tag{6}$$

where the polar coordinates (ρ, ϕ) such that $x = \rho\cos\phi = \rho c_\phi$ and $y = \rho\sin\phi = \rho s_\phi$ are introduced. Hence, by means of simple algebraic manipulations, it is possible to write

$$\underline{\underline{\mathbf{J}}}(u, v) = \begin{pmatrix} \underline{\underline{\mathbf{J}}}_x(u, v) \\ \underline{\underline{\mathbf{J}}}_y(u, v) \end{pmatrix} = \frac{1}{2\pi j} \sum_{n=-\infty}^{+\infty} j^n \begin{pmatrix} c_\psi & -js_\psi \\ s_\psi & jc_\psi \end{pmatrix} \underline{\underline{\mathbf{J}}}^{(n)}(w)e^{jn\psi}, \tag{7}$$

where $u = w\cos\psi$ and $v = w\sin\psi$, and the following definition of VHT of the order n (VHT _{n}) of the n -th azimuthal harmonic of the surface current density is introduced:

$$\underline{\underline{\mathbf{J}}}^{(n)}(w) = \begin{pmatrix} \underline{\underline{\mathbf{J}}}_C^{(n)}(w) \\ -j\underline{\underline{\mathbf{J}}}_D^{(n)}(w) \end{pmatrix} = \int_0^{+\infty} \underline{\underline{\mathbf{H}}}^{(n)}(w\rho) \begin{pmatrix} J_\rho^{(n)}(\rho) \\ -jJ_\phi^{(n)}(\rho) \end{pmatrix} \rho d\rho = \int_0^{+\infty} \underline{\underline{\mathbf{H}}}^{(n)}(w\rho) \underline{\underline{\mathbf{J}}}^{(n)}(\rho) \rho d\rho, \tag{8}$$

with

$$\underline{\underline{\mathbf{H}}}^{(n)}(w\rho) = \begin{pmatrix} J_n'(w\rho) & \frac{nJ_n(w\rho)}{w\rho} \\ \frac{nJ_n(w\rho)}{w\rho} & J_n'(w\rho) \end{pmatrix}, \tag{9}$$

where $J_n(\cdot)$ and $J_n'(\cdot)$ denote the n -th order, first-kind Bessel function and its first derivative. By using (7), Equation (5) can be rewritten as follows:

$$\sum_{n=-\infty}^{+\infty} e^{jn\phi} \int_0^{+\infty} \underline{\underline{\mathbf{H}}}^{(n)}(w\rho) \underline{\underline{\mathbf{G}}}(w) \underline{\underline{\mathbf{J}}}(w) dw$$

$$= -\frac{1}{4\pi^2} \begin{pmatrix} c_\phi & s_\phi \\ js_\phi & -jc_\phi \end{pmatrix} \int_0^{+\infty} \int_0^{2\pi} \underline{\underline{\mathbf{G}}}_{2,1}^{(S)}(w, \psi) e^{-j(w\rho c_\psi - \phi + w\rho_0 c_\psi - \phi_0 + R_2(w)d + R_1(w)z_0)} w dw d\psi J_{l_0}, \tag{10}$$

where $x_0 = \rho_0 c_{\phi_0}$, $y_0 = \rho_0 s_{\phi_0}$, and

$$\underline{\underline{\mathbf{G}}}(w) = w^2 \begin{pmatrix} B_{2,2}^{(P)}(w) + B_{2,2}^{(S)}(w)e^{-j2R_2(w)d} & 0 \\ 0 & A_{2,2}^{(P)}(w) + A_{2,2}^{(S)}(w)e^{-j2R_2(w)d} \end{pmatrix}. \tag{11}$$

2.2. Proposed Solution

By virtue of Helmholtz decomposition, the surface current density on the disk can be thought of as the superposition of a surface curl-free contribution and a surface divergence-free contribution [32]. As a result, the n -th azimuthal harmonic of the surface current density can be rewritten as follows:

$$\underline{\underline{\mathbf{J}}}(n)(\rho) = \underbrace{\begin{pmatrix} d/d\rho \\ n/\rho \end{pmatrix} \Phi_C^{(n)}(\rho)}_{\underline{\underline{\mathbf{J}}}_C^{(n)}(\rho)} - j \underbrace{\begin{pmatrix} n/\rho \\ d/d\rho \end{pmatrix} \Phi_D^{(n)}(\rho)}_{\underline{\underline{\mathbf{J}}}_D^{(n)}(\rho)}, \tag{12}$$

where $\Phi_T^{(n)}(\cdot)$ with $T = C, D$ are suitable scalar potential functions.

Despite what happens to the cylindrical components of $\underline{\underline{\mathbf{J}}}(n)(\rho)$, the VHT $_n$ of $\underline{\underline{\mathbf{J}}}_T^{(n)}(\rho)$ are scalar functions [33], i.e.,

$$\begin{pmatrix} \underline{\underline{\mathbf{J}}}_C^{(n)}(w) \\ 0 \end{pmatrix} = \int_0^{+\infty} \underline{\underline{\mathbf{H}}}^{(n)}(w\rho) \underline{\underline{\mathbf{J}}}_C^{(n)}(\rho) \rho d\rho, \tag{13a}$$

$$\begin{pmatrix} 0 \\ \underline{\underline{\mathbf{J}}}_D^{(n)}(w) \end{pmatrix} = \int_0^{+\infty} \underline{\underline{\mathbf{H}}}^{(n)}(w\rho) \underline{\underline{\mathbf{J}}}_D^{(n)}(\rho) \rho d\rho, \tag{13b}$$

or, equivalently,

$$\underline{\underline{\mathbf{J}}}_T^{(n)}(w) = \int_0^{+\infty} J_n(w\rho) \Phi_T^{(n)}(\rho) w \rho d\rho, \tag{14}$$

thus suggesting $\underline{\underline{\mathbf{J}}}_T^{(n)}(\rho)$ as new unknowns in the spatial domain in order to manage scalar unknowns in the spectral domain.

The discretization of the integral equation in (10) is provided by using the Galerkin method. For this purpose, the following complete and non-redundant expansions of the scalar unknowns in the spectral domain of the orthonormal eigenfunctions of the most singular part of the integral operator that allow the reconstruction of the physical behavior of the surface current density are considered [34]:

$$\underline{\underline{\mathbf{J}}}_T^{(n)}(w) = \sum_{h=-1+\delta_{n,0}}^{+\infty} \gamma_{T,h}^{(n)} \underline{\underline{\mathbf{f}}}_T^{(n,h)}(w), \tag{15}$$

where

$$\underline{\underline{\mathbf{f}}}_T^{(n,h)}(w) = \int_0^{+\infty} J_n(w\rho) f_T^{(n,h)}(\rho) w \rho d\rho = \sqrt{2(|n| + 2h + p_T + 1)} \frac{J_{|n|+2h+p_T+1}(aw)}{w^{p_T}}, \tag{16}$$

and where $f_T^{(n,h)}(\rho)$ denote the expansion functions of $\Phi_T^{(n)}(\cdot)$, $p_C = 3/2$ and $p_D = 1/2$ in order to reconstruct the appropriate edge behavior of the surface current density, and the condition

$$\gamma_{D,-1}^{(n)} = \alpha^{(n)} \gamma_{C,-1}^{(n)}, \tag{17}$$

where $\alpha^{(n)} = j \frac{a \operatorname{sgn}(n)}{\sqrt{4n^2-1}}$, has to be verified to guarantee the vanishing of the reconstructed current for $\rho > a$.

Simple algebraic manipulations, the Galerkin method, the orthogonality property of the azimuthal harmonics, and the extraction of the most singular part of the integral operator allow the recasting of the integral equation in (10) as the following second-kind matrix equation:

$$\mathbf{x}^{(n)} + \mathbf{A}^{(n)} \mathbf{x}^{(n)} = \mathbf{c}^{(n)}, \tag{18}$$

where, by setting $\hat{\alpha}^{(n)} = \frac{1}{\sqrt{1+(k_2 \alpha^{(n)})^2}}$, the unknown vector is

$$\mathbf{x}^{(n)} = \begin{bmatrix} \frac{1}{\sqrt{2\omega\epsilon_2}} \mathbf{x}_C^{(n)} \\ \sqrt{\frac{\omega\mu_2}{2}} \mathbf{x}_D^{(n)} \end{bmatrix}, \tag{19a}$$

$$\mathbf{x}_C^{(n)} = \left\{ x_{C,h}^{(n)} \right\}_{h=-1+\delta_{n,0}}^{+\infty}, \tag{19b}$$

$$\mathbf{x}_D^{(n)} = \left\{ x_{D,h}^{(n)} \right\}_{h=0}^{+\infty} \tag{19c}$$

$$x_{C,-1}^{(n)} = \frac{\gamma_{C,-1}^{(n)}}{\hat{\alpha}^{(n)}} \text{ for } n \neq 0, \tag{19d}$$

$$x_{T,h}^{(n)} = \gamma_{T,h}^{(n)} \text{ for } h > 0, \tag{19e}$$

the coefficient matrix is

$$\mathbf{A}^{(n)} = \begin{bmatrix} -j2\omega\epsilon_2 \mathbf{A}_{C,C}^{(n)} & -2j\sqrt{\frac{\epsilon_2}{\mu_2}} \mathbf{A}_{C,D}^{(n)} \\ 2j\sqrt{\frac{\epsilon_2}{\mu_2}} \mathbf{A}_{D,C}^{(n)} & j\frac{2}{\omega\epsilon_2} \mathbf{A}_{D,D}^{(n)} \end{bmatrix}, \tag{20a}$$

$$\mathbf{A}_{C,C}^{(n)} = \left\{ A_{C,C,k,h}^{(n)} \right\}_{k,h=-1+\delta_{n,0}}^{+\infty}, \tag{20b}$$

$$\mathbf{A}_{C,D}^{(n)} = \left\{ A_{C,D,k,h}^{(n)} \right\}_{k=-1+\delta_{n,0}, h=0}^{+\infty} \tag{20c}$$

$$\mathbf{A}_{D,C}^{(n)} = \left\{ A_{D,C,k,h}^{(n)} \right\}_{k=0, h=-1+\delta_{n,0}}^{+\infty} \tag{20d}$$

$$\mathbf{A}_{D,D}^{(n)} = \left\{ A_{D,D,k,h}^{(n)} \right\}_{k,h=0}^{+\infty} \tag{20e}$$

$$A_{C,C,-1,-1}^{(n)} = \left(\hat{\alpha}^{(n)} \right)^2 \left[M_{C,-1,-1}^{(n)} - \left(\alpha^{(n)} \right)^2 M_{D,-1,-1}^{(n)} \right] \text{ for } n \neq 0, \tag{20f}$$

$$A_{C,C,-1,h}^{(n)} = A_{C,C,h,-1}^{(n)} = \hat{\alpha}^{(n)} M_{C,-1,h}^{(n)} \text{ for } n \neq 0, h \geq 0, \tag{20g}$$

$$A_{C,C,k,h}^{(n)} = A_{C,C,h,k}^{(n)} = M_{C,k,h}^{(n)} \text{ for } k, h \geq 0, \tag{20h}$$

$$A_{C,D,-1,h}^{(n)} = -A_{D,C,h,-1}^{(n)} = -\hat{\alpha}^{(n)} \alpha^{(n)} M_{D,-1,h}^{(n)} \quad \text{for } n \neq 0, h \geq 0, \tag{20i}$$

$$A_{C,D,k,h}^{(n)} = A_{D,C,h,k}^{(n)} = 0 \quad \text{for } k, h \geq 0, \tag{20j}$$

$$A_{D,D,k,h}^{(n)} = A_{D,D,h,k}^{(n)} = M_{D,k,h}^{(n)} \quad \text{for } k, h \geq 0, \tag{20k}$$

$$M_{C,k,h}^{(n)} = \int_0^{+\infty} \left(w^2 B_{2,2}^{(P)}(w) - j \frac{w}{2\omega\epsilon_2} \right) \tilde{f}_C^{(n,k)}(w) \tilde{f}_C^{(n,h)}(w) w dw + \int_0^{+\infty} w^2 B_{2,2}^{(S)}(w) e^{-j2R_2(w)d} \tilde{f}_C^{(n,k)}(w) \tilde{f}_C^{(n,h)}(w) w dw, \tag{20l}$$

$$M_{D,k,h}^{(n)} = \int_0^{+\infty} \left(w^2 A_{2,2}^{(P)}(w) + j \frac{\omega\mu_2}{2w} \right) \tilde{f}_D^{(n,k)}(w) \tilde{f}_D^{(n,h)}(w) w dw + \int_0^{+\infty} w^2 A_{2,2}^{(S)}(w) e^{-j2R_2(w)d} \tilde{f}_D^{(n,k)}(w) \tilde{f}_D^{(n,h)}(w) w dw, \tag{20m}$$

and the free term is

$$\mathbf{c}^{(n)} = \begin{bmatrix} j \frac{1}{\sqrt{2\omega\epsilon_2}} \mathbf{c}_C^{(m)} \\ -j \sqrt{\frac{\omega\mu_2}{2}} \mathbf{c}_D^{(m)} \end{bmatrix}, \tag{21a}$$

$$\mathbf{c}_C^{(n)} = \{c_{C,k}^{(n)}\}_{k=-1+\delta_{n,0}}^{+\infty}, \tag{21b}$$

$$\mathbf{c}_D^{(n)} = \{c_{D,k}^{(n)}\}_{k=0}^{+\infty}, \tag{21c}$$

$$c_{C,-1}^{(n)} = \hat{\alpha}^{(n)} (b_{C,-1}^{(n)} - \alpha^{(n)} b_{D,-1}^{(n)}) \quad \text{for } n \neq 0, \tag{21d}$$

$$c_{T,k}^{(n)} = b_{T,k}^{(n)} \quad \text{for } k > 0, \tag{21e}$$

$$b_{C,k}^{(n)} = -\frac{e^{-jn\phi_0}}{2\pi} \int_0^{+\infty} \left\{ \frac{1}{2} w^2 B_{2,1}^{(S)}(u, v) \left[(J_{0x} - jJ_{0y}) e^{j\phi_0} J_{n-1}(w\rho_0) - (J_{0x} + jJ_{0y}) e^{-j\phi_0} J_{n+1}(w\rho_0) \right] \right. \\ \left. - jw C_{2,1}^{(S)}(u, v) J_{0z} J_n(w\rho_0) \right\} e^{-j(R_2(w)d + R_1(w)z_0)} \tilde{f}_C^{(n,k)}(w) w dw, \tag{21f}$$

$$b_{D,k}^{(n)} = -j \frac{e^{-jn\phi_0}}{2\pi} \int_0^{+\infty} \frac{1}{2} w^2 A_{2,1}^{(S)}(u, v) \left[(J_{0x} - jJ_{0y}) e^{j\phi_0} J_{n-1}(w\rho_0) \right. \\ \left. + (J_{0x} + jJ_{0y}) e^{-j\phi_0} J_{n+1}(w\rho_0) \right] e^{-j(R_2(w)d + R_1(w)z_0)} \tilde{f}_D^{(n,k)}(w) w dw, \tag{21g}$$

for each n integer number. Following the reasoning proposed by the authors in [33] and the references therein, both the compactness of the matrix operator $\mathbf{A}^{(n)}$ in l^2 and the l^2 -norm boundedness of the free term $\mathbf{c}^{(n)}$ can be demonstrated. As a result, according to Fredholm theory, the existence of the solution originates from its uniqueness, and the approximate solution obtained by truncating the matrix equation in (18) converges to the exact solution as the truncation order tends to infinity.

3. Numerical Results

Of course, the coefficient matrix and the free term elements of the Fredholm second-kind equation in (18) have to be numerically evaluated. To this purpose, it is worth observing that since the integrands of the second integral in (20l) and (20m) and of the

integrals in (21f) and (21g) are asymptotically exponentially decaying functions, the corresponding integrals quickly converge. On the other hand, the first integral in (20l) and the first integral in (20m), which are improper integrals of oscillating functions with an asymptotic algebraic decay, can be rewritten as combinations of fast-converging proper integrals by means of an analytical procedure in the complex plane proposed by the authors in a previous paper [26]. Henceforth, the numerical simulations were provided by means of in-house C++ software code running on a laptop equipped with an Intel Core i7-10510U 1.8 GHz processor and 16 GB of RAM, and the integrals were evaluated by means of an adaptive scheme based on a 24-point Gauss–Legendre quadrature rule.

The fast convergence of the proposed method can be quantified by introducing the following normalized truncation error:

$$\text{err}(M, N) = \sqrt{\frac{\sum_{n=-N+1}^{N-1} \|\mathbf{x}_{M+1}^{(n)} - \mathbf{x}_M^{(n)}\|^2}{\sum_{n=-N+1}^{N-1} \|\mathbf{x}_M^{(n)}\|^2}}, \tag{22}$$

where the symbols $\|\cdot\|$ and $\mathbf{x}_M^{(n)}$ denote, respectively, the Euclidean norm and the vector of the first M expansion coefficients for each unknown, whereas $2N - 1$ is the number of azimuthal harmonics used. It can be shown that the convergence rate is slightly affected by the disk depth and the position and orientation of the dipole. However, as expected, it is affected by the disk radius in terms of both the number of expansion functions and azimuthal harmonics to be used in order to achieve a predetermined accuracy. Such behavior is shown in Figure 2a,b, where the normalized truncation error is plotted as a function of M for $N = 7$ and as a function of N for $M = 8$ for a zero-thickness PEC disk of radius $a = 5, 10, 15, 20$ cm buried in a lossy half-space with $\epsilon_{r2} = 3.5 - j0.3$ and $\mu_{r2} = 1$ at a depth $d = 3$ cm, and illuminated by a Hertzian dipole directed along the y axis with $|J_0| = 10^{-3}$ Am, operating at 800 MHz and located in the upper half-space filled by air, $\epsilon_{r1} = \mu_{r1} = 1$, at $x_0 = -2$ m, $y_0 = 2$ m, $z_0 = 2$ m. It is worth noting that $M = 8$ and $N = 7$ achieved a normalized truncation error less than 10^{-3} for the worst case examined, i.e., for $a = 20$ cm, with a computation time of 50 s.

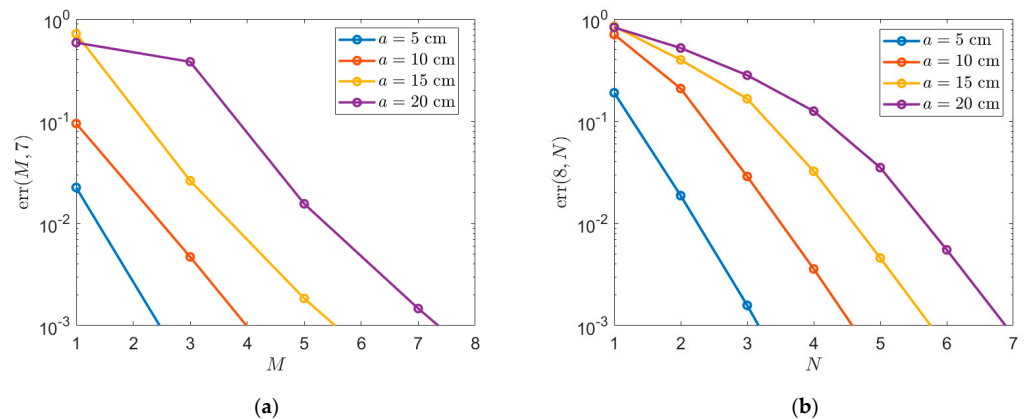


Figure 2. Normalized truncation error for a zero-thickness PEC disk of radius $a = 5, 10, 15, 20$ cm buried in a lossy half-space with $\epsilon_{r2} = 3.5 - j0.3$ and $\mu_{r2} = 1$ at a depth $d = 3$ cm, and illuminated by a Hertzian dipole directed along the y axis with $|J_0| = 10^{-3}$ Am, operating at 800 MHz and located in air, $\epsilon_{r1} = \mu_{r1} = 1$, at $x_0 = -2$ m, $y_0 = 2$ m, $z_0 = 2$ m, as a function of (a) M for $N = 7$ and as a function of (b) N for $M = 8$.

Validation of the developed in-house C++ software code was carried out by means of comparisons with CST-MWS. To this purpose, it must be emphasized that the commercial software was not designed to deal with scattering problems involving layered media, thus

forcing an approximation of the infinite layered medium to a finite one. Unfortunately, a fairly accurate solution can be obtained only when a very large, with respect to the wavelength, layered region is involved, with an exorbitant number of mesh-cells and an endless computation time to perform the simulations. For this reason, comparisons are provided only in homogeneous medium, in particular, even when medium 2 in Figure 1 is filled with air, i.e., $\epsilon_{r1} = \mu_{r1} = \epsilon_{r2} = \mu_{r2} = 1$. In Figure 3, the amplitude of the components of the surface current density on a zero-thickness PEC disk of radius $a = 10$ cm, located at $d = 3$ cm, and illuminated by a Hertzian dipole directed along the y axis with $|J_0| = 10^{-3}$ Am, operating at 800 MHz and located at $x_0 = -2$ m, $y_0 = 2$ m, $z_0 = 2$ m, is plotted along the x and y axes, i.e., for $|x/a| \leq 1$, $y = 0$, and for $x = 0$, $|y/a| \leq 1$, and compared with the ones reconstructed by means of CST-MWS. The agreement is excellent. However, the proposed method achieved a normalized truncation error less than 10^{-3} for $M = 4$ and $N = 5$ with a computation time of 15 s, whereas the time-domain solver of CST-MWS required about 30 million mesh-cells with a computation time of about 3 h to accurately reconstruct the solution.

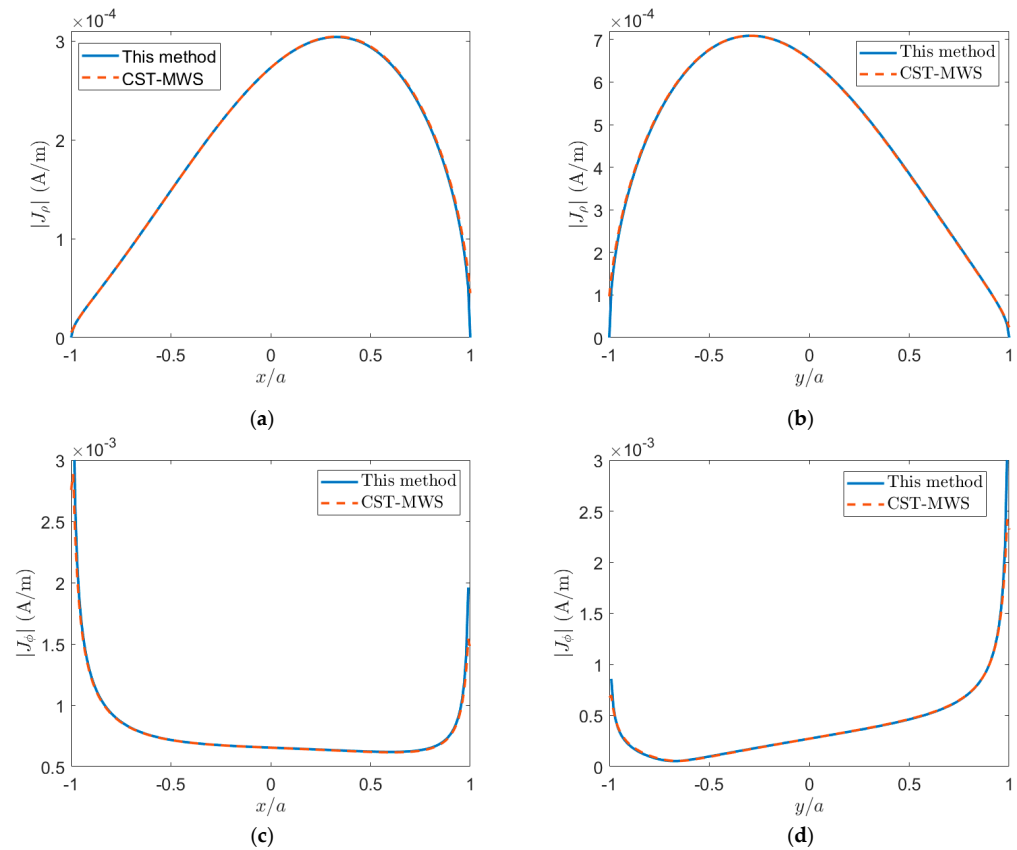


Figure 3. Amplitude of the components of the surface current density along the x and y axes on a zero-thickness PEC disk of radius $a = 10$ cm, located at $d = 3$ cm, and illuminated by a Hertzian dipole directed along the y axis with $|J_0| = 10^{-3}$ Am, operating at 800 MHz and located at $x_0 = -2$ m, $y_0 = 2$ m, $z_0 = 2$ m, for $\epsilon_{r1} = \mu_{r1} = \epsilon_{r2} = \mu_{r2} = 1$. (a) $|J_\rho|$ along the x axis, (b) $|J_\rho|$ along the y axis, (c) $|J_\phi|$ along the x axis, and (d) $|J_\phi|$ along the y axis. Blue solid line: this method; red dashed line: CST-MWS.

As an example of the application of the proposed method, a configuration was considered that resembled a measurement system of the field scattered from a landmine based on a two drones, one equipped with a transmitting antenna and the other equipped with a receiving antenna. As with the cases examined before, a zero-thickness PEC disk, of radius $a = 10$ cm buried in a lossy half-space with $\epsilon_{r2} = 3.5 - j0.3$ and $\mu_{r2} = 1$ at the depth $d = 3$ cm, was considered. Now, the transmitting Hertzian dipole, directed

along the y axis with $|J_0| = 10^{-3} \text{Am}$ and operating at 800 MHz, was located in the upper half-space filled by air, $\epsilon_{r1} = \mu_{r1} = 1$, at $z_0 = 2 \text{ m}$ and four different positions in the xy plane: (1) $x_0 = -2 \text{ m}$, $y_0 = 2 \text{ m}$, (2) $x_0 = 0 \text{ m}$, $y_0 = 2 \text{ m}$, (3) $x_0 = -2 \text{ m}$, $y_0 = 0 \text{ m}$, and (4) $x_0 = 0 \text{ m}$, $y_0 = 0 \text{ m}$. The scattered field was evaluated in the horizontal area $(x, y) \in [-2 \text{ m}, 2 \text{ m}] \times [-2 \text{ m}, 2 \text{ m}]$ for $z = 1 \text{ m}$. In Figure 4, two separate plots for the amplitudes of the incidence and the scattered electric fields in the area of interest are provided for the four cases examined. In the figures, the disk circumference is denoted by the black dotted circular line. Clearly, the reflection due to the discontinuity interface between the two involved media perturbs the classical spherical wave behavior of the field radiated by the dipole in a homogeneous medium. On the other hand, the disk “footprint” is clearly observable in the scattered field behavior. As a matter of fact, the bright spot (in yellow) is elliptical with a maximum shifted in the opposite direction with respect to the dipole position, except, of course, for the last case examined, in which the dipole is along the disk axis.

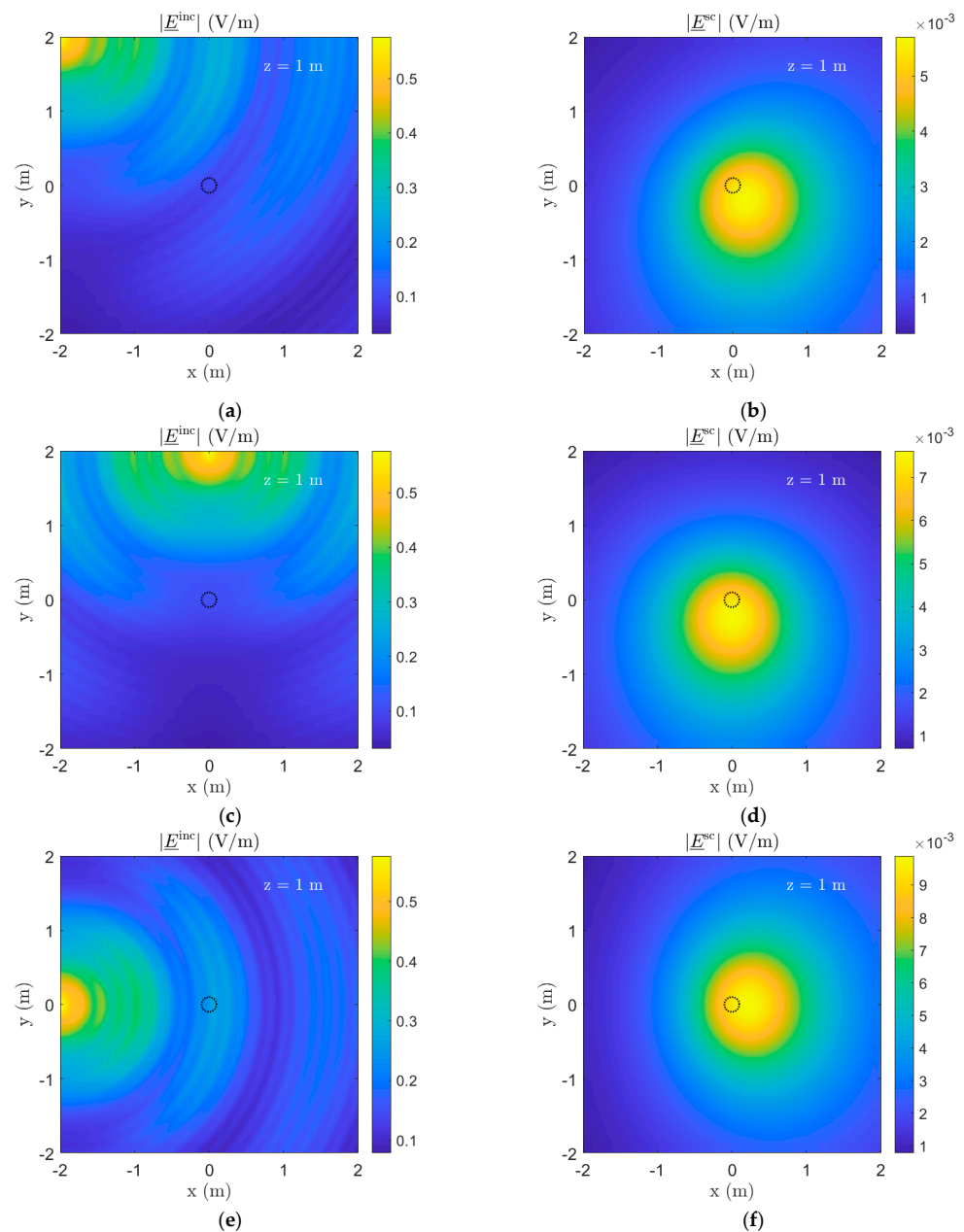


Figure 4. Cont.

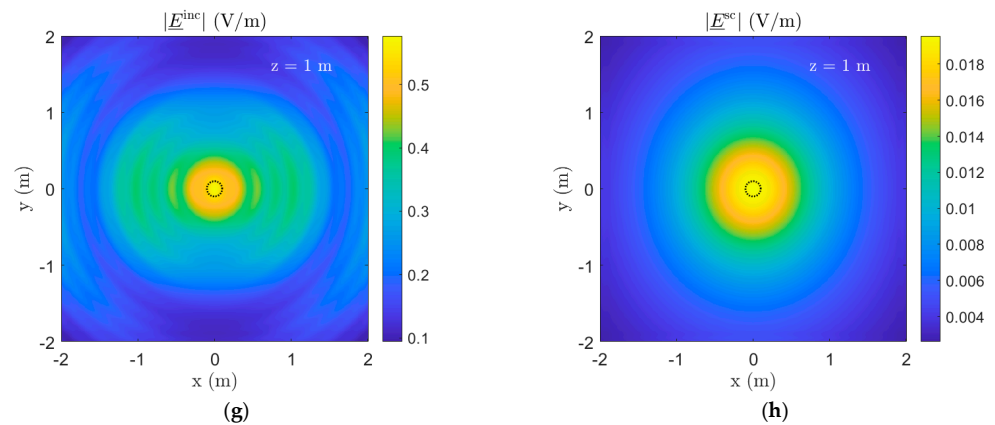


Figure 4. Amplitudes of the incident and scattered electric fields in the horizontal area $(x, y) \in [-2 \text{ m}, 2 \text{ m}] \times [-2 \text{ m}, 2 \text{ m}]$ for $z = 1 \text{ m}$ in the case of a zero-thickness PEC disk of radius $a = 10 \text{ cm}$ buried in a lossy half-space with $\epsilon_{r2} = 3.5 - j0.3$ and $\mu_{r2} = 1$ at a depth $d = 3 \text{ cm}$, and illuminated by a Hertzian dipole directed along the y axis with $|J_0| = 10^{-3} \text{ Am}$, operating at 800 MHz and located in the upper half-space filled by air, $\epsilon_{r1} = \mu_{r1} = 1$, at $z_0 = 2 \text{ m}$, and 4 different positions in the xy plane: (a,b) $x_0 = -2 \text{ m}$, $y_0 = 2 \text{ m}$; (c,d) $x_0 = 0 \text{ m}$, $y_0 = 2 \text{ m}$; (e,f) $x_0 = -2 \text{ m}$, $y_0 = 0 \text{ m}$; and (g,h) $x_0 = 0 \text{ m}$, $y_0 = 0 \text{ m}$. The black dotted circular line denotes the disk circumference.

4. Conclusions

In this paper, an analysis of the dipole field scattering from a zero-thickness PEC disk buried in a lossy half-space has been carried out by generalizing the guaranteed-convergence Helmholtz–Galerkin technique proposed by the authors in previous papers for dealing with plane-wave scattering from a disk and a holed plane in a homogeneous medium. The advantage of using this method is twofold. First, convergence of the method to the exact solution of the problem is guaranteed due to the Fredholm second-kind nature of the obtained matrix equation. Second, the convergence is very fast because the unknowns are expanded by means of functions reconstructing the physical behavior of the fields. As a matter of fact, the proposed numerical results demonstrate that the numerical resources, in terms of both computation time and memory occupation, to achieve highly accurate results are paltry and drastically less than those required by CST-MWS. Therefore, the proposed method can be particularly suitable for the implementation of effective inverse scattering iterative algorithms. Moreover, it can serve as a reference for the validation of general-purpose commercial software without a mathematically guaranteed convergence.

Author Contributions: Conceptualization, M.L. and M.D.M.; methodology, M.L.; software, M.L.; validation, G.A.C.; formal analysis, M.L.; data curation, G.C. and D.P.; writing—original draft preparation, M.L., M.D.M. and F.S.; writing—review and editing, M.L., G.A.C., M.D.M. and F.S.; supervision, M.L.; funding acquisition, M.D.M. All authors have read and agreed to the published version of the manuscript.

Funding: This research was partially funded by the Italian Ministry of University and Research (MUR) under the Program for the Development of Research of National Interest (PRIN) 2022 “TERRAIN”, CUP H53D23007300001, funded by the EU in the NextGenerationEU plan.

Institutional Review Board Statement: Not applicable.

Informed Consent Statement: Not applicable.

Data Availability Statement: The data presented in this study were obtained by means of in-house software code implementing the proposed method and by using the commercial software CST Microwave Studio 2023.

Conflicts of Interest: The authors declare no conflicts of interest.

References

1. Robledo, L.; Carrasco, M.; Mery, D. A survey of land mine detection technology. *Int. J. Remote Sens.* **2009**, *30*, 2399–2410. [[CrossRef](#)]
2. Amiri, A.; Tong, K.; Chetty, K. Feasibility study of multi-frequency ground penetrating radar for rotary UAV platforms. In Proceedings of the IET International Conference on Radar Systems, Glasgow, UK, 22–25 October 2012.
3. Colorado, J.; Perez, M.; Mondragon, I.; Mendez, D.; Parra, C.; Devia, C.; Martinez-Moritz, J.; Neira, L. An integrated aerial system for landmine detection: SDR-based ground penetrating radar onboard an autonomous drone. *Adv. Robot.* **2017**, *31*, 791–808. [[CrossRef](#)]
4. Sipos, D.; Planinsic, P.; Gleich, D. On drone ground penetrating radar for landmine detection. In Proceedings of the IEEE 1st International Conference on Landmine, Detection, Clearance Legislations, Beirut, Lebanon, 26–28 April 2017.
5. Ferrara, V.; Pietrelli, A.; Chicarella, S.; Pajewski, L. GPR/GPS/IMU system as buried objects locator. *Measurements* **2018**, *114*, 534–541. [[CrossRef](#)]
6. García Fernández, M.; Álvarez López, Y.; Arboleya Arboleya, A.; González Valdés, B.; Rodríguez Vaqueiro, Y.; Las-Heras Andrés, F.; Pino García, A. Synthetic aperture radar imaging system for landmine detection using a Ground Penetrating Radar on board a Unmanned Aerial Vehicle. *IEEE Access* **2018**, *6*, 45100–45112. [[CrossRef](#)]
7. Pinchera, D.; Migliore, M.D. Efficient synthesis of concentric-rings plane wave generators. *IEEE Trans. Antennas Propag.* **2023**, *71*, 4967–4975. [[CrossRef](#)]
8. O'Neill, K.; Haider, S.A.; Geimer, S.D.; Paulsen, K.D. Effects of the ground surface on polarimetric features of broadband radar scattering from subsurface metallic objects. *IEEE Trans. Geosci. Remote Sens.* **2001**, *39*, 1556–1565. [[CrossRef](#)]
9. Demarest, K.; Plumb, R.; Huang, Z. FDTD modeling of scatterers in stratified media. *IEEE Trans. Antennas Propag.* **1995**, *43*, 1164–1168. [[CrossRef](#)]
10. Huang, Z.; Demarest, K.R.; Plumb, R.G. An FDTD/MoM hybrid technique for modeling complex antennas in the presence of heterogeneous grounds. *IEEE Trans. Geosci. Remote Sens.* **1999**, *37*, 2692–2698. [[CrossRef](#)]
11. Cui, T.J.; Chew, W.C. Fast algorithm for electromagnetic scattering by buried conducting plates of large size. *IEEE Trans. Antennas Propag.* **1999**, *47*, 1116–1118. [[CrossRef](#)]
12. Zhuang, L.; He, S.Y.; Ye, X.B.; Hu, W.D.; Yu, W.X.; Zhu, G.Q. The BCGS-FFT method combined with an improved discrete complex image method for EM scattering from electrically large objects in multilayered media. *IEEE Trans. Geosci. Remote Sens.* **2010**, *48*, 1180–1185. [[CrossRef](#)]
13. Losada, V.; Boix, R.R.; Medina, F. Fast and accurate algorithm for the short-pulse electromagnetic scattering from conducting circular plates buried inside a lossy dispersive half-space. *IEEE Trans. Geosci. Remote Sens.* **2003**, *41*, 988–997. [[CrossRef](#)]
14. Alcuntu, Y.; Yapar, A.; Akduman, I. On the scattering of electromagnetic waves by bodies buried in a half-space with locally rough interface. *IEEE Trans. Geosci. Remote Sens.* **2006**, *44*, 1435–1443.
15. Hongo, K.; Jafri, A.D.U.; Naqvi, Q.A. Scattering of electromagnetic spherical wave by a perfectly conducting disk. *Prog. Electromagn. Res.* **2012**, *129*, 315–343. [[CrossRef](#)]
16. Balaban, M.V.; Sauleau, R.; Garcia-Vigueras, M.; Nosich, A.I. Terahertz range elementary dipole excitation of a thin dielectric disk sandwiched between two graphene covers: Integral equation analysis. In Proceedings of the IEEE International Conference on Microwaves, Antennas, Communications and Electronic Systems (COMCAS), Tel-Aviv, Israel, 4–6 November 2019.
17. Herasymova, D.O.; Dukhopelnykov, S.V.; Lucido, M.; Nosich, A.I. Optical sensing of electron-beam position with twin silver nanotube antenna tuned to hybrid surface plasmon resonance. *IEEE J. Sel. Top. Quantum Electron.* **2021**, *27*, 4601008. [[CrossRef](#)]
18. Kantorovich, L.V.; Akilov, G.P. *Functional Analysis*, 2nd ed.; Pergamon/Oxford-Elmsford: New York, NY, USA, 1982.
19. Tsalamengas, J.L. Exponentially converging Nystrom's methods for systems of singular integral equations with applications to open/closed strip- or slot-loaded 2-D structures. *IEEE Antennas Propag. Mag.* **2006**, *54*, 1549–1558. [[CrossRef](#)]
20. Bulygin, V.S.; Nosich, A.I.; Gandel, Y.V. Nystrom-type method in three-dimensional electromagnetic diffraction by a finite PEC rotationally symmetric surface. *IEEE Trans. Antennas Propag.* **2012**, *60*, 4710–4718. [[CrossRef](#)]
21. Bulygin, V.S.; Benson, T.M.; Gandel, Y.V.; Nosich, A.I. Full-wave analysis and optimization of a TARA-like shield-assisted paraboloidal reflector antenna using Nystrom-type method. *IEEE Trans. Antennas Propag.* **2013**, *61*, 4981–4989. [[CrossRef](#)]
22. Lucido, M.; Schettino, F.; Migliore, M.D.; Pinchera, D.; Di Murro, F.; Panariello, G. Electromagnetic scattering by a zero-thickness PEC annular ring: A new highly efficient MoM solution. *J. Electromagn. Waves Appl.* **2017**, *31*, 405–416. [[CrossRef](#)]
23. Lucido, M.; Balaban, M.V.; Nosich, A.I. Terahertz-range plasmon and whispering gallery mode resonances in the plane wave scattering from thin microsize dielectric disk with graphene covers. *Proc. Math. Phys. Eng. Sci.* **2022**, *478*, 2262. [[CrossRef](#)]
24. Lucido, M.; Nosich, A.I. Analytical regularization approach to plane wave diffraction from circular hole in infinite resistive plane. *IEEE Trans. Antennas Propag.* **2023**, *71*, 6878–6892. [[CrossRef](#)]
25. Chew, W.C.; Kong, J.A. Resonance of nonaxial symmetric modes in circular microstrip disk antenna. *J. Math. Phys.* **1980**, *21*, 2590–2598. [[CrossRef](#)]
26. Lucido, M.; Di Murro, F.; Panariello, G. Electromagnetic scattering from a zero-thickness PEC disk: A note on the Helmholtz-Galerkin analytically regularizing procedure. *Progr. Electromagn. Res. Lett.* **2017**, *71*, 7–13. [[CrossRef](#)]
27. Chew, W.C. *Waves and Fields in Inhomogeneous Media*; IEEE Press: Piscataway, NJ, USA, 1995.
28. Chew, W.C.; Chen, S.Y. Response of a point source embedded in a layered medium. *IEEE Antennas Wirel. Propag. Lett.* **2003**, *2*, 254–258. [[CrossRef](#)]

29. Michalski, K.A.; Zheng, D. Rigorous analysis of open microstrip lines of arbitrary cross section in bound and leaky regimes. *IEEE Trans. Microw. Theory Tech.* **1989**, *37*, 2005–2010. [[CrossRef](#)]
30. Meixner, J. The behavior of electromagnetic fields at edges. *IEEE Trans. Antennas Propag.* **1972**, *20*, 442–446. [[CrossRef](#)]
31. Makarov, G.I.; Osipov, A.V. Structure of Meixner's series. *Radiophys. Quantum Electron.* **1986**, *29*, 544–549. [[CrossRef](#)]
32. Van Bladel, J. A discussion of Helmholtz' theorem on a surface. *Arch. Elektron. Ubertrag.* **1993**, *47*, 131–136.
33. Lucido, M.; Balaban, M.V.; Dukhopelnykov, S.V.; Nosich, A.I. A fast-converging scheme for the electromagnetic scattering from a thin dielectric disk. *Electronics* **2020**, *9*, 1451. [[CrossRef](#)]
34. Wilkins, J.E. Neumann series of Bessel functions. *Trans. Am. Math. Soc.* **1948**, *64*, 359–385. [[CrossRef](#)]

Disclaimer/Publisher's Note: The statements, opinions and data contained in all publications are solely those of the individual author(s) and contributor(s) and not of MDPI and/or the editor(s). MDPI and/or the editor(s) disclaim responsibility for any injury to people or property resulting from any ideas, methods, instructions or products referred to in the content.